Chapter 6
Wave-Smart Absorption: A Parametric Study of Dashpot Location in Beam Structures

Samikhshak Gupta, Abigail Smith, and Vijaya V. N. Sriram Malladi

Abstract Flexural waveguides carry vibration as traveling waves that are partly reflected and absorbed at local impedance changes. Characterizing these interactions through frequency-dependent power reflection and absorption coefficients, $\rho(\omega)$ and $\alpha(\omega)$, is critical for structurally efficient vibration control. We present a wave-energy framework for optimally placing a compact passive absorber—a spring–damper (dashpot)—to maximize $\alpha(\omega)$. Broadband excitation is introduced with a piezoelectric actuator, and spatiotemporal responses are captured using scanning laser Doppler vibrometry (SLDV). Sensor spacing is selected to suppress evanescent content, ensuring the analysis isolates propagating waves that dominate in large, lightweight structures. An undamped host-beam baseline isolates the absorber's effect, while wave-amplitude decomposition provides $\rho(\omega)$ and $\alpha(\omega)$. Parametric sweeps map α versus absorber location and frequency. A repeatable pattern emerges: peak absorption occurs at multiple placements repeating at odd quarter-wavelength intervals—velocity antinodes—along the waveguide. With increasing frequency (shorter wavelength), the number of absorption peaks grows, reflecting the harmonic nature of the response. These results yield a practical design rule: placing the absorber at $(2n + 1)\lambda/4$ achieves strong absorption without the mass cost of blanket damping. The resulting location–frequency map operationalizes this rule and highlights sensitivities near node–antinode transitions. Together with sensor-placement guidelines that suppress evanescent effects, the framework provides concise, wave-informed rules for passive vibration reduction and sets the stage for extensions to transmission modeling, multi-absorber layouts, and broadband absorption.

Keywords Wave-decomposition · Passive-absorber · Power-absorption · Sensor-layout · Dashpot-location

Introduction

Many structural elements, such as beams, plates, pipes, and stiffeners, act as waveguides that carry vibration as traveling waves [1]. Irregularities [2]—joints [3, 4], fasteners, material transitions [5], cracks [6], and added hardware—scatter energy and alter global response, yet their effective properties remain difficult to characterize. Uncertain boundary data limit the applicability of analytical and numerical models, while finite-element simulations often require highly accurate inputs. Conventional damping layers can reduce vibration but impose prohibitive weight costs in transportation [7] and aerospace applications [7]. These challenges motivate experimental, wave-based strategies that act locally at interfaces. Within this framework, the absorption coefficient, derived from reflection and transmission, provides an energy-based and experimentally accessible measure to characterize discontinuities and guide lightweight vibration control [8, 9].

Dynamic vibration absorbers (DVAs) provide a practical means of tailoring impedance. Passive devices are reliable and straightforward, but they are inherently narrowband. Semi-active and active devices [10–21, 21–26] introduce adaptability through actuators and control but at the cost of added complexity, expense, and potential stability issues [27]. Hybrid approaches often pair a passive baseline with active or semi-active augmentation. Although DVAs are widely used in machinery, vehicles, and buildings, the role of absorber placement in governing wave absorption remains underexplored.

Samikhshak Gupta · Abigail Smith · Vijaya V. N. Sriram Malladi
Vibrations, Intelligent Testing, & Active Learning of Structures (ViTALS) Group, Department of Mechanical and Aerospace Engineering, Michigan Technological University, Houghton, MI 49931
e-mail: sgupta14@mtu.edu; abrsmith@mtu.edu; smalladi@mtu.edu

Kristin B. Zimmerman, PhD (eds.), *Structural Health Monitoring, Metamaterials, Metastructures and Additive Manufacturing and Dynamics of Biomedical and Bioinspired Systems, 2026, Vol. 10*, Conference Proceedings of the Society for Experimental Mechanics Series, https://doi.org/10.1007/978-8-743-81449-8_6

This study adopts a purely passive approach [28–33], employing a compact spring–damper (Airpot 2KS160) mounted on a beam, with spanwise location as the design variable. Relocating the dashpot modifies local mobility and interface impedance, thereby influencing reflection and absorption. Wave decomposition is used to extract reflection and absorption coefficients, and parametric studies establish the relationship between dashpot placement and absorption. The results demonstrate how location-dependent impedance can be leveraged to maximize absorption at target frequencies, providing a lightweight, wave-informed strategy for vibration reduction.

Numerical Model & Wave Decomposition

A beam made of Al 6061-T6 with a rectangular cross-section of $19.05\,\mathrm{mm} \times 1.5875\,\mathrm{mm}$ and a length of $1.113\,\mathrm{m}$ is considered in this study. Using the Timoshenko beam formulation, the governing equations are described as

$$\begin{aligned} GA\kappa\left(\frac{\partial\psi(x,t)}{\partial x} - \frac{\partial^2\psi(x,t)}{\partial x^2}\right) + \rho A\frac{\partial^2 y(x,t)}{\partial t^2} &= q(x,t), \\ GA\kappa\left(\frac{\partial y(x,t)}{\partial x} - \psi(x,t)\right) + EI\frac{\partial^2\psi(x,t)}{\partial x^2} &= \rho I\frac{\partial^2 y(x,t)}{\partial t^2}\ , \end{aligned} \tag{1}$$

where G is the shear modulus, A is the area of cross-section, $y(x,t)$ and $\psi(x,t)$ are the transverse displacement and the bending rotation angle at location x and time t, q is the load, E is the Young's Modulus, ρ is the density, and I is the moment of inertia. This section provides a concise overview of the modeling approach used to analyze a beam incorporating a spring-damper (SD) system that functions as a passive absorber (PA). The schematic representation of the clamped-clamped beam, incorporating a discrete spring-damper with stiffness denoted by the stiffness is denoted by k $[\mathrm{N\,m^{-1}}]$ and the damping coefficient by c $[\mathrm{N-s/m}]$. The beam is driven by a harmonic point load $F(t) = F_0 e^{\mathrm{i}\omega t}$ applied near the right clamp ($x \approx 0.88 \times L$). Clamped boundaries at $x = 0$ and $x = L$ impose $y(0,t) = y(L,t) = 0$ and $\psi(0,t) = \psi(L,t) = 0$. A MATLAB-based FE-model comprising 400 quadratic shape functions has been thoroughly tested and validated in previous research endeavors [34–37] using the equation of motion as,

$$\mathbf{M}\ddot{\mathbf{x}} + \mathbf{C}\dot{\mathbf{x}} + \mathbf{K}\mathbf{x} = B_f F(t) \tag{2}$$

where the mass, damping, and stiffness matrices are denoted as $\mathbf{M}, \mathbf{C}, \mathbf{K} \in \mathbb{R}^{1598\times1598}$. A proportional (Rayleigh) damping model is adopted, allowing C to be expressed as a linear combination of $\mathbf{M}$ and $\mathbf{K}$ [35, 38–41], as

$$\mathbf{C} = \alpha\mathbf{M} + \beta\mathbf{K} \tag{3}$$

where $\alpha = 0.7099\mathrm{s}^{-1}$ and $\beta = 8.8166e^{-8}\mathrm{s}$ are finite element constants determined experimentally. In particular, a thorough analysis shows that the natural frequencies converged within the applicable frequency range. The spring–damper assembly is positioned at $L_0 = 0.0988L$, and the corresponding modeshapes are shown in Figure 1.

MATLAB is utilized to solve the equation of motion Equation (4) employing the inverse matrix technique;

$$\mathbf{M}\ddot{\mathbf{x}} + (\mathbf{C} + cB_{sd})\,\dot{\mathbf{x}} + (\mathbf{K} + kB_{sd})\,\mathbf{x} = B_f F(t) \tag{4}$$

where $\mathbf{x}$ is the displacement vector; $\mathbf{M}$, $\mathbf{C}$, and $\mathbf{K}$ are the assembled mass, damping, and stiffness matrices; k and c parameterize the SD stiffness and damping; $F(t)$ denotes an excitation applied near the far end; B_f distributes the external force; and B_{sd} distributes the SD interaction [42]. The parameters k and c are optimized, subject to specified bounds, to maximize the absorption coefficient at a selected frequency. Consider the same beam model with a spring–damper system—akin to an acoustic black hole—attached at $L_0 = 0.0988L$. For a given frequency, the Timoshenko-beam wavenumber follows from the dispersion relation as

$$\frac{EI}{\rho A}{k_f}^4 - \frac{I}{A}\left(1 + \frac{E}{G\kappa}\right){k_f}^2\omega^2 - \omega^2 + \frac{\rho I}{GA\kappa}\omega^4 = 0\,. \tag{5}$$

Here, κ is the Timoshenko correction factor; ω the angular frequency; ρ the density; E the Young's modulus; G the shear modulus; A the cross-sectional area; and I the second moment of area. Because the solution for k_f depends quadratically on ω, the beam exhibits dispersion. The resulting response by superposition [43, 44] is written as,

$$\mathbf{W}(x,t) = \left(\underbrace{\tilde{A}\,e^{-\iota k_f x}}_{\substack{\text{forward}\\ \text{propagating}}} + \underbrace{\tilde{B}\,e^{+\iota k_f x}}_{\substack{\text{backward}\\ \text{propagating}}} + \underbrace{\tilde{C}\,e^{-k_f x}}_{\substack{\text{forward}\\ \text{evanescent}}} + \underbrace{\tilde{D}\,e^{+k_f x}}_{\substack{\text{backward}\\ \text{evanescent}}} + \underbrace{\cdots}_{\text{higher–order modes}}\right) e^{\mathrm{i}\omega t}\ . \tag{6}$$

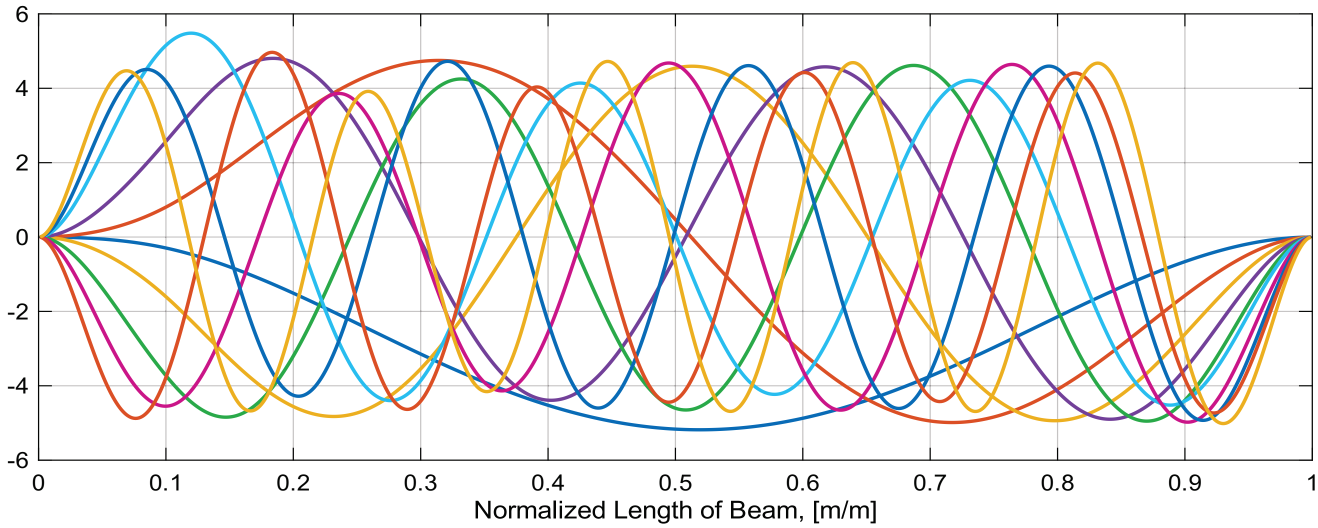

Fig. 1 Modeshapes of the host beam with a dashpot attached at the end

In the above expression, k_f is the spatial frequency obtained from Equation (5) at the chosen ω. Although a solution exists for each ω_n, the explicit summation over frequencies is suppressed for clarity [44]; see [45] for a spectral treatment of wave propagation. Neglecting noise and nonlinear higher-order terms, the sensor measurement $\mathbf{W}(x_i,t)$ at position x_i is a local instance of the field:

$$\mathbf{W}(x_i,t) = \left(\tilde{A}\,e^{-\iota k_f x_i} + \tilde{B}\,e^{+\iota k_f x_i} + \tilde{C}\,e^{k_f x_i} + \tilde{D}\,e^{k_f x_i}\right) e^{\mathrm{i}\omega t}.$$

Applying a Fast Fourier Transform (FFT) at x_i yields, for each frequency,

$$\mathbf{W}(x_i) = \tilde{A}(\omega)\,e^{-\iota k_f x_i} + \tilde{B}(\omega)\,e^{+\iota k_f x_i} + \tilde{C}(\omega)\,e^{k_f x_i} + \tilde{D}(\omega)\,e^{k_f x_i}\,. \tag{7}$$

In Equation (7), the wavenumber k_f is obtained from the Timoshenko model using known material and geometric properties, and the sensor position x_i is assumed measurable (constraints discussed later). Each measurement thus involves four unknown complex amplitudes, $\tilde{A}, \tilde{B}, \tilde{C}, \tilde{D} \in \mathbb{C}$, which describe the modal content of the field. To streamline wave amplitude estimation, we neglect evanescent terms by adopting a far-field placement of sensors—evanescent contributions are strongest near boundaries/discontinuities and the sources of excitation—and by selecting sensor locations accordingly. The ensuing constraints specify dashpot placement and sensor spacing to suppress evanescent effects, enforce wavelength-based separation between adjacent sensors, and respect practical experimental limitations for future tests.

Table 1 Constraints for Sensor Placement

	Constraint Condition	**Result**
Far-Field Assumption	$\mathrm{e}^{-k_f\,l} = 0.1,\ \forall\,\omega \in [0.775,\ 20]$ kHz	$l = 0.05\,\mathrm{m}$
Wavelength-Based Spacing	$\Delta_{\max} < \dfrac{\lambda_{\min}}{2}$	$\Delta_{\max} = 0.012\,\mathrm{m}$
Experimental Spacing	$\Delta_{\min} >$ SLDV spatial resolution	$\Delta_{\min} = 0.009\,\mathrm{m}$

Table 1 summarizes the placement rules used to suppress evanescent components. To treat evanescent terms as negligible, the response is required to decay by 90% over the propagation distance l from the source [46]; accordingly, sensors are placed at least $l = 0.05\,\mathrm{m}$ from boundaries, the dashpot, and the excitation point. To avoid spatial aliasing, inter-sensor spacing follows the half-wavelength criterion across the bandwidth of interest [4]. With $\lambda_{\min}$ attained at $f_{\max} = 20\,\mathrm{kHz}$, the allowable spacing is $\Delta_{\max} = 0.012\,\mathrm{m}$. Finally, a practical resolution limit for future SLDV measurements sets a minimum spacing of $\Delta_{\min} = 0.009\,\mathrm{m}$. Also, to avoid high condition numbers while doing the inverse problem, a non-uniform sensor layout is adopted [47, 48].

For the end-mounted dashpot case in Figure 2, we assume no transmission and only reflection to simplify the analysis. At $x = x_0$, the response is expressed through a decomposition that isolates positive- and negative-going wave amplitudes.

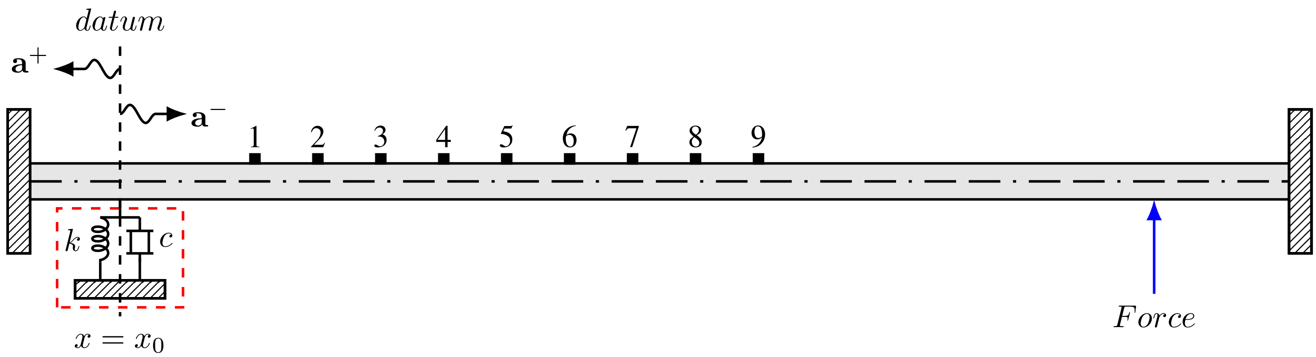

Fig. 2 Schematic Diagram of a clamped–clamped beam with a spring-damper at an end

The responses measured by the n sensors (displacement, velocity, or acceleration) are represented as $\mathbf{W} = \Lambda\mathbf{A}$, where

$$\mathbf{W} = \begin{Bmatrix} \mathbf{W}(x_1) \\ \mathbf{W}(x_2) \\ \vdots \\ \mathbf{W}(x_n) \end{Bmatrix}, \Lambda = \begin{bmatrix} e^{-\iota k_f x_1} & e^{\iota k_f x_1} \\ e^{-\iota k_f x_2} & e^{\iota k_f x_2} \\ \vdots & \vdots \\ e^{-\iota k_f x_n} & e^{\iota k_f x_n} \end{bmatrix}, \mathbf{A} = \begin{Bmatrix} a_p^+ \\ a_p^- \end{Bmatrix} . \tag{8}$$

Because the sensors are positioned to suppress evanescent/near-field terms, only the propagating amplitudes $a_p^{\pm}$ remain, with $+$ and $-$ signs denoting positive and negative propagation. $\mathbf{W}(x_i)$ is the measured output at $x = x_i$ for $i = 1, 2, \cdots, n$. Although two sensors suffice, here $n = 9$ are used so the same beam model accommodates future cases with multiple dashpots. For implementation, we express $\mathbf{W}(x_i)$ as the acceleration-to-force transfer function, rather than in terms of spatial displacement; the resulting wave amplitudes are accelerations per unit force, which does not alter the reflection or transmission coefficients. Wave amplitudes are reconstructed from measurements of $\mathbf{W}$ via

$$\mathbf{A} = \Lambda^{-1}\mathbf{W}, \quad \mathbf{A} = (\Lambda^{\mathrm{H}}\Lambda)^{-1}\Lambda^{\mathrm{H}}\mathbf{W} ,$$

for square and overdetermined systems, respectively. The reflection coefficient is then defined by,

$$r_p = \frac{a_p^-}{a_p^+} . \tag{9}$$

Because the phase terms in Equation (9) are sensitive to errors in k_f and the datum–sensor distances, accordingly, this study focuses on the power coefficients in Equations (10) and (11). The power reflection coefficient is defined as,

$$\rho = |r_p|^2 , \tag{10}$$

and the corresponding power absorption coefficient is shown as.

$$\alpha = 1 - |r_p|^2, \quad or \quad \alpha = 1 - \rho . \tag{11}$$

Figures 3a and 3b show the reflection and power-reflection coefficients, respectively. When propagation coefficients are included in the damping model, the plots reveal appreciable structural damping: even without a passive damper, the power absorption coefficient $\alpha(\omega)$ in Figure 3c remains nonzero across the band. To avoid conflating intrinsic material damping with added damping, we therefore adopt an undamped host-beam model in which $\rho(\omega) = 1$ and $\alpha(\omega) = 0$, as indicated by the black dotted curves in Figures 4b and 4c. These figures also show that introducing a dashpot alters both ρ and α, confirming that a spring–damper modifies the beam's absorption characteristics. Building on this result, the next section examines how relocating the dashpot along the beam affects the power absorption coefficient.

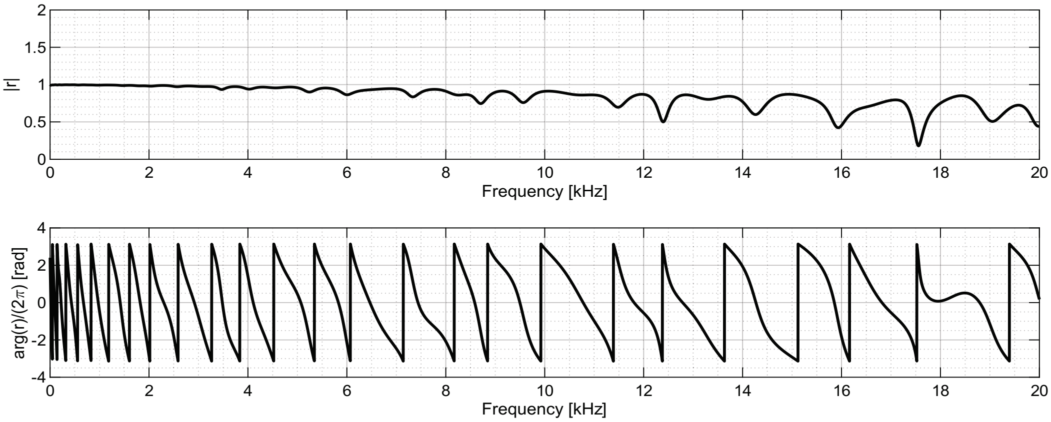

(a) Magnitude & phase of reflection coefficient for the host beam

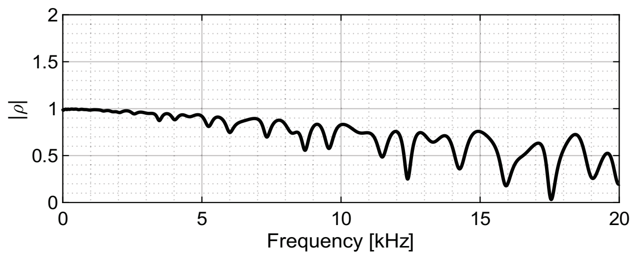

(b) Power reflection coefficient magnitude

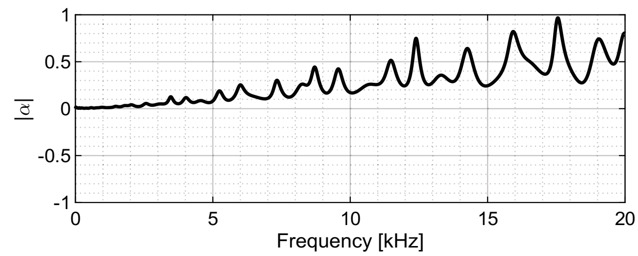

(c) Power absorption coefficient magnitude

Fig. 3 Wave-amplitude coefficients for the host beam with a proportional damping model

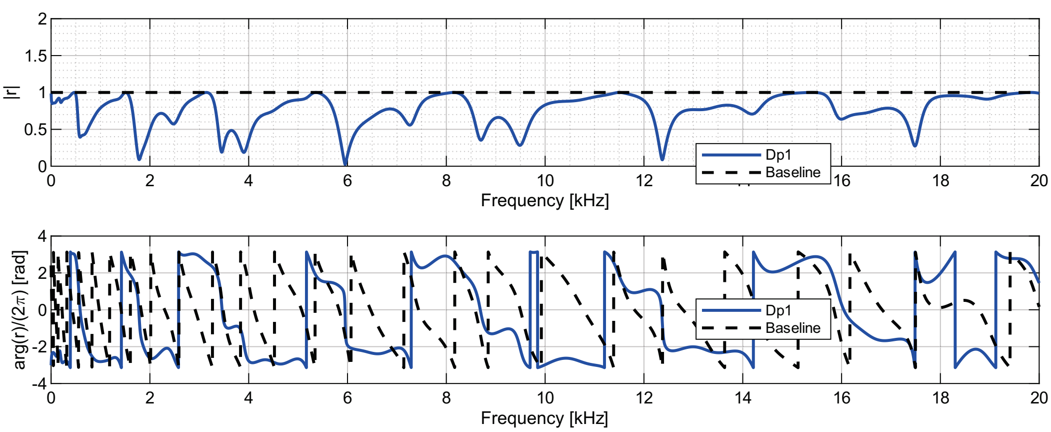

(a) Magnitude and phase of the reflection coefficient for the undamped host beam with a dashpot attached at the end

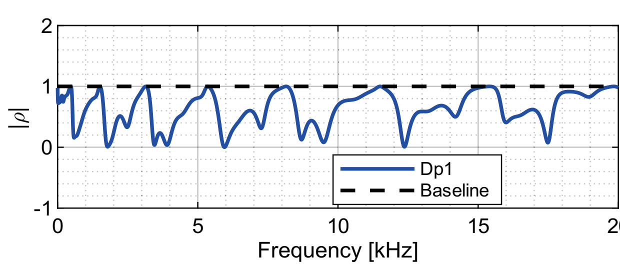

(b) Power reflection coefficient magnitude for the undamped host beam with a dashpot attached at the end

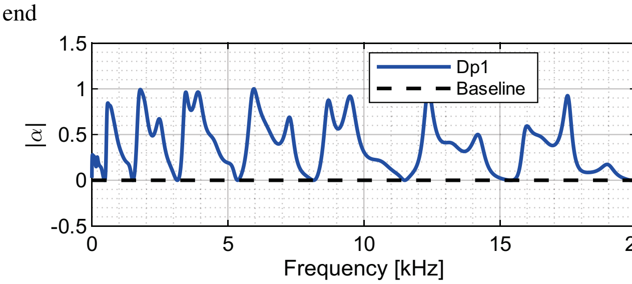

(c) Power absorption coefficient magnitude for the undamped host beam with a dashpot attached at the end.

Fig. 4 Wave amplitude coefficients for the undamped host beam with a dashpot attached at the end

Results

The results in Figures 4b and 4c indicate that adding a spring–damper alters both ρ and α, highlighting its impact on the beam's absorption behavior. We next assess how relocating the dashpot along the span affects the power absorption coefficient. At a fixed frequency, $\alpha(\omega)$ depends on both the damping coefficient and the passive absorber (PA) location; to isolate location effects, the damping coefficient is set to the value that maximizes α at that frequency. The PA is then swept from 0.017 m to 0.149 m measured from a clamped end, under the maintained assumption of no transmission. The spring–damper properties used in this sweep are held constant and reported in Table 2. It is evident from Figure 5a that, at the

Table 2 Spring-Damper Properties

Frequency	Damping Coefficient	Wavelength	Number of Peaks
(a) 2940 Hz	$29.06\,\mathrm{N-s/m}$	$\lambda_1 = 0.07\,\mathrm{m}$	*4*
(b) 11623 Hz	$41.02\,\mathrm{N-s/m}$	$\lambda_2 = 0.035\,\mathrm{m}$	*7*

single tuning frequency 2940 Hz, multiple dashpot locations deliver peak absorption for the same damping coefficient—i.e., optimal placement is not unique. At 2940 Hz the wavelength is $\lambda_1 = 0.07$ m. Halving it to $\lambda_2 = 0.035$ m (so $\lambda_2 \simeq \lambda_1/2$) and applying the dispersion relation yields a corresponding frequency of 11623 Hz, as listed in Table 2. At this higher frequency, the number of absorption peaks increases from 4 to 7 (see Figure 5b), consistent with the harmonic character of the power absorption coefficient: when the wavelength is halved, the spatial peak pattern approximately doubles, and the principal peaks of the power absorption coefficient align with harmonic wavelength scaling.

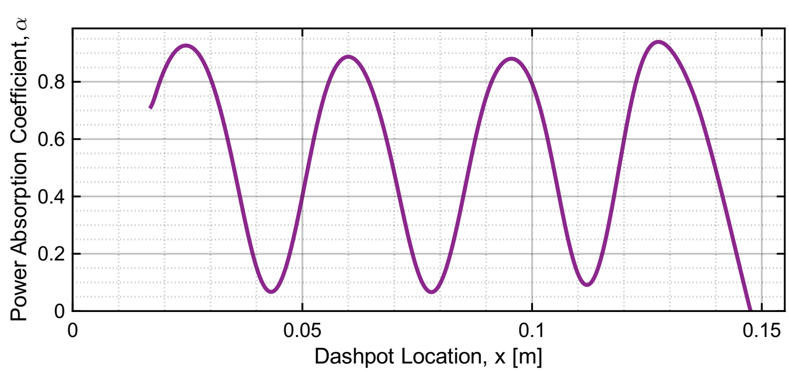

(a) Power Absorption v/s Dashpot Location where dashpot is tuned at 2940 Hz

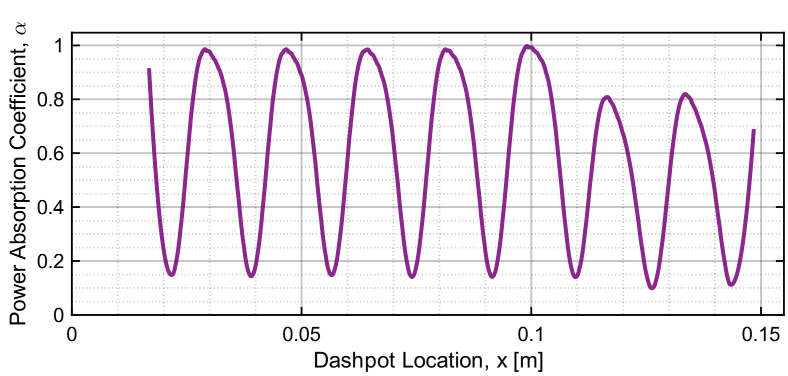

(b) Power Absorption v/s Dashpot Location where dashpot is tuned at 11623 Hz

Fig. 5 Power Absorption v/s Dashpot Location

Conclusion

This work introduced a wave-based strategy for positioning a compact spring–damper on a beam to maximize power absorption. Establishing an undamped baseline—$\rho(\omega) = 1$, $\alpha(\omega) = 0$—isolated the absorber's influence and showed that adding a dashpot markedly reshapes both the power reflection and absorption coefficients. Parametric sweeps then quantified how α varies with spanwise location. A simple, repeatable pattern emerges: optimal placements are not unique but repeat at approximately half-wavelength intervals, and halving the wavelength (i.e., moving to higher frequency via the dispersion relation) increases the number of absorption peaks, consistent with the harmonic nature of the response.

In practice, these results lead to a clear placement rule: maximum absorption occurs when the dashpot is positioned at the vibration antinodes, which lie at odd quarter-wavelengths from the clamped end.

$$\text{Dashpot Location} = \frac{(2n+1)\lambda}{4}, \quad n = 0, 1, 2, \ldots$$

Placing the absorber at velocity antinodes maximizes vibration absorption while avoiding the mass penalty of blanket damping. This rule yields broad regions of effective placement but also heightened sensitivity near node–antinode transitions, where small shifts in position can markedly change α. Paired with sensor-placement guidelines that suppress evanescent content, the method offers an experimentally grounded, wave-informed route to lightweight vibration reduction. A natural next step is to include transmission to generalize the coefficients and capture through-energy paths. Coordinating multiple absorbers—passive, semi-active, or active—can broaden impedance control, and SLDV hardware tests will assess robustness to modeling and boundary uncertainties. Overall, the results provide concise, wave-informed placement rules and a path to scalable, mass-efficient vibration control in structural waveguides.

Acknowledgments The authors (VVNSM and SG) would like to thank the support of the National Science Foundation through the grant CMMI-2301776 for sponsoring the research presented in this paper.

Declaration of generative AI and AI-assisted technologies in the writing process

While preparing this work, the author(s) used ChatGPT to edit the language. After using this tool/service, the author(s) reviewed and edited the content as needed and take(s) full responsibility for the publication's content.

References

1. Cremer, L., Heckl, M., Ungar, E., et al. "Structure-borne sound". *Journal of Applied Mechanics*, 41(3):839 (1974)
2. Wexler, A. "Solution of waveguide discontinuities by modal analysis". *IEEE Transactions on Microwave Theory and Techniques*, 15(9):508–517 (2003)
3. Muggleton, J., Waters, T., Mace, B., and Zhang, B. "Approaches to estimating the reflection and transmission coefficients of discontinuities in waveguides from measured data". *Journal of sound and vibration*, 307(1-2):280–294 (2007)
4. Zhang, B., Waters, T.P., and Mace, B.R. "Identifying joints from measured reflection coefficients in beam-like structures with application to a pipe support". *Mechanical Systems and Signal Processing*, 24(3):784–795 (2010)
5. Suchoski Jr, P. and Ramaswamy, V. "Exact numerical technique for the analysis of step discontinuities and tapers in optical dielectric waveguides". *Journal of the Optical Society of America A*, 3(2):194–203 (1986)
6. Fan, Q., Gao, Q., Huang, Z., and Ji, L. "Crack detection in an infinite beam based on the amplitudes of the wave reflection coefficients".
7. Rastegar, N., Ershad-Langroudi, A., Parsimehr, H., and Moradi, G. "Sound-absorbing porous materials: a review on polyurethane-based foams". *Iranian Polymer Journal*, 31(1):83–105 (2022)
8. Liu, G., Cai, C., and Lam, K. "Sound reflection and transmission of compliant plate-like structures by a plane sound wave excitation". *Journal of sound and vibration*, 230(4):809–824 (2000)
9. Russell, D.A. "Absorption coefficients and impedance". *Science and Mathematics Department. GMI Engineering & Management Institute Flint, MI*, 48504 (1999)
10. Herold, S. and Mayer, D. "Adaptive piezoelectric absorber for active vibration control". In *actuators*, volume 5, page 7. MDPI (2016)
11. Hollkamp, J.J. and Starchville Jr, T.F. "A self-tuning piezoelectric vibration absorber". *Journal of intelligent material systems and structures*, 5(4):559–566 (1994)
12. Chen, Y.D., Fuh, C.C., and Tung, P.C. "Application of voice coil motors in active dynamic vibration absorbers". *IEEE Transactions on magnetics*, 41(3):1149–1154 (2005)
13. Yan, Z., Li, G., Luo, J., Zeng, J., Zhang, W., Wang, Y., Yang, W., and Ma, G. "Vibration control of superconducting electro-dynamic suspension train with electromagnetic and sky-hook damping methods". *Vehicle system dynamics*, 60(10):3375–3397 (2022)
14. Olgac, N. and Holm-Hansen, B. "A novel active vibration absorption technique: delayed resonator". *Journal of sound and vibration*, 176(1):93–104 (1994)
15. Petitjean, B. and Legrain, I. "Feedback controllers for active vibration suppression". *Journal of Structural Control*, 3(1-2):111–127 (1996)
16. Behrens, S., Fleming, A., and Moheimani, S. "A broadband controller for shunt piezoelectric damping of structural vibration". *Smart materials and structures*, 12(1):18 (2003)

17. Pietrzko, S. and Mao, Q. “Reduction of structural sound radiation and vibration using shunt piezoelectric materials”. *Solid State Phenomena*, 147:882–889 (2009)
18. Gardonio, P. and Rodrigues, G.K. “Shunted piezoelectric patch adaptive vibration absorber set to maximise electric power absorption: A comparison between parallel and series rl-shunts”. *Journal of Vibration and Control*, 31(1-2):37–50 (2025)
19. Heuss, O., Salloum, R., Mayer, D., and Melz, T. “Tuning of a vibration absorber with shunted piezoelectric transducers”. *Archive of Applied Mechanics*, 86(10):1715–1732 (2016)
20. Niederberger, D., Morari, M., and Pietrzko, S.J. “Adaptive resonant shunted piezoelectric devices for vibration suppression”. In *Smart Structures and Materials 2003: Smart Structures and Integrated Systems*, volume 5056, pages 213–224. SPIE (2003)
21. Berardengo, M., Høgsberg, J., Manzoni, S., Vanali, M., Brandt, A., and Godi, T. “Lrlc-shunted piezoelectric vibration absorber”. *Journal of Sound and Vibration*, 474:115268 (2020)
22. Guyomar, D. and Badel, A. “Nonlinear semi-passive multimodal vibration damping: An efficient probabilistic approach”. *Journal of sound and vibration*, 294(1-2):249–268 (2006)
23. Badel, A., Sebald, G., Guyomar, D., Lallart, M., Lefeuvre, E., Richard, C., and Qiu, J. “Piezoelectric vibration control by synchronized switching on adaptive voltage sources: Towards wideband semi-active damping”. *The Journal of the Acoustical Society of America*, 119(5):2815–2825 (2006)
24. Elahinia, M., Ciocanel, C., Nguyen, T.M., and Wang, S. “Mr-and er-based semiactive engine mounts: A review”. *Smart Materials Research*, 2013(1):831017 (2013)
25. Holdhusen, M.H. and Cunefare, K.A. “Damping effects on the state-switched absorber used for vibration suppression”. *Journal of Intelligent Material Systems and Structures*, 14(9):551–561 (2003)
26. Walsh, P.L. and Lamancusa, J. “A variable stiffness vibration absorber for minimization of transient vibrations”. *Journal of sound and vibration*, 158(2):195–211 (1992)
27. Xu, Z. “Study on adaptive tuned vibration absorbing technology”. *PhD diss., University of Science and Technology of China* (2010)
28. Baz, A. and Ro, J. “Vibration control of plates with active constrained layer damping”. *Smart materials and structures*, 5(3):272 (1996)
29. Gupta, A., Panda, S., and Reddy, R.S. “Damping capabilities of viscoelastic composites for active/passive constrained layer damping of the plate vibration: a comparative study”. *Journal of Vibration Engineering & Technologies*, 12(1):891–908 (2024)
30. Mohammed, A.D. “Development of a four arms viscoelasic damper and its application to a heavy floor vibration due to walking excitation”.
31. Mantellato, R., Pertile, M., Colombatti, G., Valmorbida, A., and Lorenzini, E. “Two-bar model for free vibrations damping of space tethers by means of spring-dashpot devices”. *CEAS Space Journal*, 6(3):133–143 (2014)
32. Xu, Z., Wang, M.Y., and Chen, T. “A particle damper for vibration and noise reduction”. *Journal of Sound and Vibration*, 270(4-5):1033–1040 (2004)
33. Matlack, K.H., Bauhofer, A., Krödel, S., Palermo, A., and Daraio, C. “Composite 3d-printed metastructures for low-frequency and broadband vibration absorption”. *Proceedings of the National Academy of Sciences*, 113(30):8386–8390 (2016)
34. Albakri, M.I., Malladi, V.V.S., Gugercin, S., and Tarazaga, P.A. “Estimating dispersion curves from frequency response functions via vector-fitting”. *Mechanical Systems and Signal Processing*, 140:106597 (2020)
35. Malladi, V.V.S., Albakri, M., and Tarazaga, P.A. “An experimental and theoretical study of two-dimensional traveling waves in plates”. *Journal of Intelligent Material Systems and Structures*, 28(13):1803–1815 (2017)
36. Malladi, V.V.S., Albakri, M.I., Krishnan, M., Gugercin, S., and Tarazaga, P.A. “Estimating experimental dispersion curves from steady-state frequency response measurements”. *Mechanical Systems and Signal Processing*, 164:108218 (2022)
37. Chavan, S.H., Gosavi, H.S., Malladi, S.S., and Malladi, V.V.S. “Bistable dvr meta-structure: A reinforcement learning approach to vibration control”. *Journal of Sound and Vibration*, 610:119068 (2025)
38. Kancharala, A. and Philen, M. “Enhanced hydrodynamic performance of flexible fins using macro fiber composite actuators”. *Smart materials and structures*, 23(11):115012 (2014)
39. Schwarz, B. and Richardson, M. “Proportional damping from experimental data”. In *Topics in Modal Analysis, Volume 7: Proceedings of the 31st IMAC, A Conference on Structural Dynamics, 2013*, pages 179–186. Springer (2013)
40. Adhikari, S. “Damping modelling using generalized proportional damping”. *Journal of Sound and Vibration*, 293(1-2):156–170 (2006)
41. Davaria, S., Sriram Malladi, V., and Tarazaga, P.A. “Bio-inspired nonlinear control of artificial hair cells”. In *Structural Health Monitoring, Photogrammetry & DIC, Volume 6: Proceedings of the 36th IMAC, A Conference and Exposition on Structural Dynamics 2018*, pages 179–184. Springer (2018)
42. Motaharibidgoli, S., Davaria, S., Malladi, V.V.S., and Tarazaga, P.A. “Developing coexisting traveling and standing waves in euler-bernoulli beams using a single-point excitation and a spring-damper system”. *Journal of Sound and Vibration*, 556:117728 (2023)
43. Mace, B. “Wave reflection and transmission in beams”. *Journal of sound and vibration*, 97(2):237–246 (1984)
44. Corbin, N.A. and Tarazaga, P. “Forward/backward decomposition for dispersive wave propagation measurements”. *Applied Sciences*, 15(2):858 (2025)
45. Doyle, J.F. “Wave propagation in structures”. In *Wave Propagation in Structures: An FFT-Based Spectral Analysis Methodology*, pages 126–156. Springer (1989)
46. Denis, V., Gautier, F., Pelat, A., and Poittevin, J. “Measurement and modelling of the reflection coefficient of an acoustic black hole termination”. *Journal of Sound and Vibration*, 349:67–79 (2015)
47. Halkyard, C. and Mace, B. “Structural intensity in beams—waves, transducer systems and the conditioning problem”. *Journal of Sound and Vibration*, 185(2):279–298 (1995)
48. Halkyard, C. “Sensor array design for wave decomposition in the presence of coupled motion”. *Journal of sound and vibration*, 259(4):935–953 (2003)